Micro-scale evolution of mechanical properties of glass-ceramic sealant for solid oxide fuel/electrolysis cells

M. Fakouri Hasanabadi [a,*], J. Malzbender [b], S. M. Groß-Barsnick [c], H. Abdoli [d], A. H. Kokabi [a], M. A. Faghihi-Sani [a]

[a] Department of Materials Science and Engineering, Sharif University of Technology, Azadi Avenue, P. O. Box 11155-9466, Tehran, Iran

[b] Forschungszentrum Jülich GmbH, Institute of Energy and Climate Research, IEK-2, 52425 Jülich, Germany

[c] Forschungszentrum Jülich GmbH, Central Institute of Engineering, Electronics and Analytic, ZEA-1, 52425 Jülich, Germany

[d] Department of Renewable Energy, Niroo Research Institute (NRI), P.O. Box 1466551 Tehran, Iran

E-mail addresses: hasanabadi68@gmail.com (M. Fakouri Hasanabadi), j.malzbender@fz-juelich.de (J. Malzbender), s.m.gross@fz-juelich.de (S. M. Groß-Barsnick), hamidabdoli@yahoo.com (H. Abdoli), kokabi@sharif.edu (A. H. Kokabi), faghihi@sharif.edu (M. A. Faghihi-Sani)

Abstract

The structural integrity of the sealant is critical for the reliability of solid oxide cells (SOCs) stacks. In this study, elastic modulus (E), hardness (H) and fracture toughness (K_{IC}) of a rapid crystallizing glass of BaO-CaO-SiO_2 system termed “sealant G” are reported as determined

using an indentation test method at room temperature. A wide range of indentation loads (1 mN–10 N) was used to investigate the load-dependency of these mechanical properties. Values of 95 ± 12 GPa, 5.8 ± 0.2 GPa and 1.15 ± 0.07 MPa·m$^{0.5}$ were derived for E, H and K_{IC} using the most suitable indentation loads. An application relevant annealing treatment of 500 h at 800 ºC does not lead to a significant change of the mechanical properties. Potential self-healing behavior of the sealant has also been studied by electron microscopy, based on heat treatment of samples with indentation-induced cracks for 70 h at 850 ºC. Although the sealant G is considered to be fully crystallized, evidence indicates that its cracks can be healed even in the absence of a dead load.

Keywords: Solid oxide cells; Sealant; Fracture toughness; Hardness; Elastic modulus; Self-healing.

1. Introduction

Solid oxide fuel/electrolysis cells (SOFCs/SOECs) are electrochemical devices that are capable to directly convert the chemical energy of fuels (hydrogen/hydrocarbons) into electricity and vice versa by promoting a redox reaction across a solid ceramic electrolyte [1]. The solid oxide cell (SOC) has the highest operation temperature (600 °C – 1000 °C) among all types of fuel/electrolysis cells [1]. To achieve a higher yield, individual cells are connected in series to form a stack. In the planar-type stack design, the planar cells are typically fixed and hermetically sealed in metallic housings and interconnected by metallic plates [2]. The glass-ceramics are the most favorable materials for SOC sealing applications due to their low cost, ease of fabrication and tailorable properties [3–6].

Stresses may arise during components production, joining and assembling them in a SOCs stack and also during the transportation, installation and periodic maintenance of the stacks [7]. In the case of stationary applications of solid oxide cell systems, the stack components should retain their stability and withstand numerous thermal cycles to room temperature over the stack lifetime (> 40,000 h) as a prerequisite for commercialization [8]. The exothermic/endothermic reactions in cells, as well as the flow of hot/cold gases in channels, result in temperature gradients inside the stack [7]. Usually, there is a mismatch in the coefficient of thermal expansion (*CTE*) of the joined components, which can lead to thermal stress generation at both operation and room temperatures [9]. Also, chemically-induced strains such as the irreversible expansion of Ni-based anodes during SOC operation must be added in the consideration of the thermal strains [9]. These external loads and internally generated stresses may result in cracking of weak components and loss of gas tightness, which can allow direct combustion of fuel creating hot spots [9]. Even though this is initially a local event, the generated heat can lead to the extension of a local crack into a large scale failure [9]. Therefore, a comprehensive assessment of stack components considering their mechanical behavior at different temperatures, in particular for the sealant, is necessary [10].

Regarding the presence of different loading states (dynamic or static) and stress types (normal or shear) on the stack components; various mechanical properties of sealing material have been evaluated [11–20]. Although the glass-ceramics often behave as a viscous material at operating conditions, they are completely brittle at room temperature (RT) [3]. Therefore, their shear strength (or creep resistance) and tensile strength (or fracture toughness) are critical at room and elevated temperatures, respectively [21]. Micro-scale ceramic phases are the main toughening agents of glass-ceramics [22]. Therefore, understanding their behavior on a micro-scale is necessary especially when the respective crack growth needs to be understood.

Furthermore, regarding reliability and simulation of cells and stacks knowledge of basic mechanical properties is important.

Various glass-forming systems have been considered for sealing SOCs stacks, including those ones based on phosphates, borates, and silicates. However, it has been reported that phosphate and borate glasses are not sufficiently stable in a humidified fuel gas environment, hence, tending to undergo significant corrosion through the formation of volatile species as well as reacting with other stack components and degrading them [23]. The electrical resistivity of alkaline earth metal oxide-containing glasses is generally higher than that of alkali metal oxide-containing glasses since the larger radius of alkaline earth modifier ions (such as Ba^{2+} and Ca^{2+}) results in lower ionic mobility in the glass network [24]. The alkali silicate glasses also tend to interact deleteriously with the ceramic cell materials [23]. Alkaline earth silicate glasses can also achieve a *CTE* close to the ceramic cell and metallic frame/interconnect via the use of a controlled crystallization process [25]. Therefore, Forschungszentrum Jülich has focused on glass-ceramic sealants based on the BaO-CaO-SiO_2 ternary system over the past three decades [26].

Recently, the flexural and shear strengths of a rapid crystallizing glass termed type G have been evaluated for SOC sealing applications [21,26]. The choice of this sealant was based on its high crystallization after a short joining time, which results in higher stability of its properties during operation [26]. In the current study, the indentation method is used to evaluate its elastic modulus (E), hardness (H) and fracture toughness (K_{IC}). Also, the self-healing capability of this fully crystallized glass at elevated temperatures is investigated.

2. Experimental

The investigated glass termed "G" is based on the BaO-CaO-SiO_2 ternary system modified with the minor additions, as shown in Table 1 [27]. Details on the glass production process can be found in [21]. The glass transition temperature (T_g), softening point (T_d) and crystallization peak temperature (T_p) of this glass are 657 ºC, 750 ºC and 946 ºC, respectively [27]. Typically the glass is crystallized for a fixed time (usually 10 h) at the envisaged joining temperature (850 ºC), yielding finally the material in its glass-ceramic state. The coefficient of thermal expansion (*CTE*) of material G after crystallization and in the glass-ceramic state is ~10×10^{-6} K^{-1} [27].

Table 1. Chemical composition of glass G [27].

	BaO	SiO_2	CaO	Additions
wt.%	34.5	44.0	14.9	B_2O_3, Al_2O_3

The initial glass powder with its median particle size of 10–13 μm was uniaxially cold-pressed into bar shapes, placed inside a platinum foil-covered mold, heat-treated for 10 h at 850 ºC and then cooled down to room temperature (RT). The sintered samples were ground flat to $t \times b \times L$ of $3 \times 4 \times 25$ mm^3 using a wheel type B126. In addition to as-sintered bars, some annealed bars were prepared by additional heat treatment of the as-sintered ones at 800 ºC for 500 h. Heating and cooling rates in all cases were 2 $K \cdot min^{-1}$. After heat treatments, the bars were embedded in epoxy 2000 (Cloeren Technology GmbH, Germany) and then polished with SiC papers (600 and 2000 grit), diamond pastes (from 3 to 1 μm) and 0.05 μm silica suspension consecutively.

Indentation tests were carried out to assess elastic modulus (E), hardness (H) and fracture toughness (K_{IC}). A Poisson's ratio (ν) of 0.25 was considered for the glass-ceramic in the

respective calculations [28]. Regarding the required force range for each material property, different indentation test machines were employed as shown in Table 2. The tests were carried out 21 times at each maximum indentation load (F_{max}). The value of K_{IC} was determined on the basis of the indentation crack length (ICL) method. The equations used for computing the values of E, H and K_{IC} have been presented in [29–31]. The topography of the polished surface was mapped by a scanning probe microscope (SPM) mounted on a Hysitron machine. Note, although the K_{IC} measurement on the basis of this method is still under discussion since the crack system induced by indentation testing is complex and leads to considerable residual stresses [32], it was implemented in the current work to permit a comparison of the material's behavior to values reported in previous studies [33].

Table 2. Utilized indentation test machines.

Indentation test machine	Indenter tip	Force range	Evaluated characteristics
Micromet, Buehler, USA	Vickers	3-10 N	H and K_{IC}
MH4, Koopa, Iran	Vickers	10 N	Self-healing
HC100, Fischer, Germany	Vickers	1 N	H and E
CSM, CSM instrument, Switzerland	Berkovich	10-500 mN	H and E
TI-980, Hysitron, USA	Berkovich	1 mN	H, E and surface topography

The measured E values by indention method are compared with ones that have been determined via impulse excitation (IE) and three-point bending (3PB) techniques. For this purpose, the IE and 3PB tests were carried out on both sintered and annealed bars following the procedures outlined in ASTM E1876 and DIN EN 843-2, respectively. A commercial

GrindoSonic system (Lemmens KG, Belgium) was employed for impulse excitation (IE) testing and dynamic Young's modulus *E* (Pa) was calculated with Eq. (1):

$$E = 0.9465 \left(\frac{mf_f^2}{b}\right)\left(\frac{L^3}{t^3}\right) T_1 \quad (1)$$

where f_f is the fundamental resonant frequency of bar in flexure (Hz), and *m*, *b*, *L* and *t* are the mass (g), width (mm), length (mm) and thickness (mm) of the bar, respectively, and T_1 *(t/L, v)* is a geometry correction factor.

three-point bending (3PB) test was carried out using a machine of Instron 1362 (Norwood, USA) equipped with a load cell of Interface 1210 BLR 1.5 kN (Scottsdale, USA) and a linear variable differential transducer (LVDT range ±1 mm, Sangamo, Bognor Regis, UK). The elastic modulus (*E*, MPa) value determined by the following equation:

$$E = \frac{D^3}{4\,b\,t^3} \times \frac{\Delta F}{\Delta \delta} \quad (2)$$

where ΔF and $\Delta \delta$ are the load (N) and displacement (mm) variations in the linear region of the load-displacement curve, respectively, and D = 20 mm is the center-to-center spacing between the supporting rods. The systematic uncertainty of the *E* values was calculated by propagating the precision of each term through the equations. The uncertainties of *m*, f_f, δ and *F* are ±0.1 mg, ±0.0005%, ±1.25 µm and ±0.04%, respectively. Also, dimensions of *L*, *b*, *t* and *D* are measured with an uncertainty of ±4 µm.

To investigate the self-healing behavior of the glass-ceramic, some indented bars were heat-treated for 70 h at 850 ºC. The samples were placed in the furnace as shown in Fig. 1 so that gravity can promote the viscous flow of residual glassy phase around cracks. To prevent contamination and to reduce the effect of radiation heating of surfaces, the bar was placed in a closed alumina crucible in the furnace during the heat treatment. The heat-treated samples were

subsequently gold coated and then investigated by scanning electron microscopy (SEM MIRA3, TESCAN, Czechia).

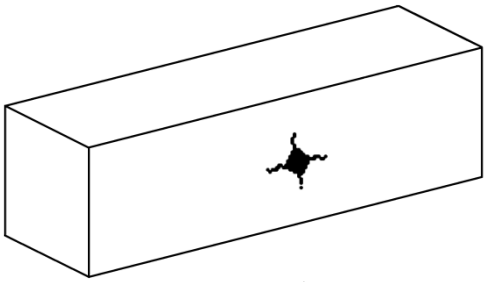

Fig. 1. Schematic of sample positioning for healing test of cracks.

3. Results and discussion

Figure 2a shows a backscattered electron (BSE) image of a zone near the edge of a bar. Three phases composed of $CaSiO_3$ (#2), $BaSi_2O_5$ (#3) and SiO_2 (#4) have been identified by analyzing the results of X-ray diffraction (XRD), energy-dispersive X-ray spectroscopy (EDS) and the relevant phase diagram [26]. Also, it has been revealed that the matrix (#1) includes $BaCa_2Si_3O_9$ and a small amount of residual glassy phase [26]. As can be seen in Fig. 2b, SiO_2 and $BaSi_2O_5$ phases have a higher resistance to abrasion, while $CaSiO_3$ was significantly abraded by the polishing material.

The results of the 21 × 21 imprint nano-indentation tests are presented as a mapping in Figs. 2c and 2d. It can be seen that the presence of different phases results in a wide range of hardness and elastic modulus values on the micro-scale. Table 3 presents the measured *H* and *E* for each phase identified for phases #1 to #4. These phases also possess different *CTE* values (Table 3), which leads to micro-stress generation during cooling from the joining/operation temperature [22]. These stresses can result in micro-cracking at the weak points or zones of stress concentration. The observations reveal that the two phases of $CaSiO_3$ and $BaSi_2O_5$ are

more prone to cracking. For example, Figs. 3a and 3b show the micro-cracks initiated from a sharp corner and created in a thin section of a $BaSi_2O_5$ phase, which can be a result of the mentioned thermal micro-stresses. The difference in density of various phases may also cause micro-stress (or even micro-porosity) generation during crystallization [34].

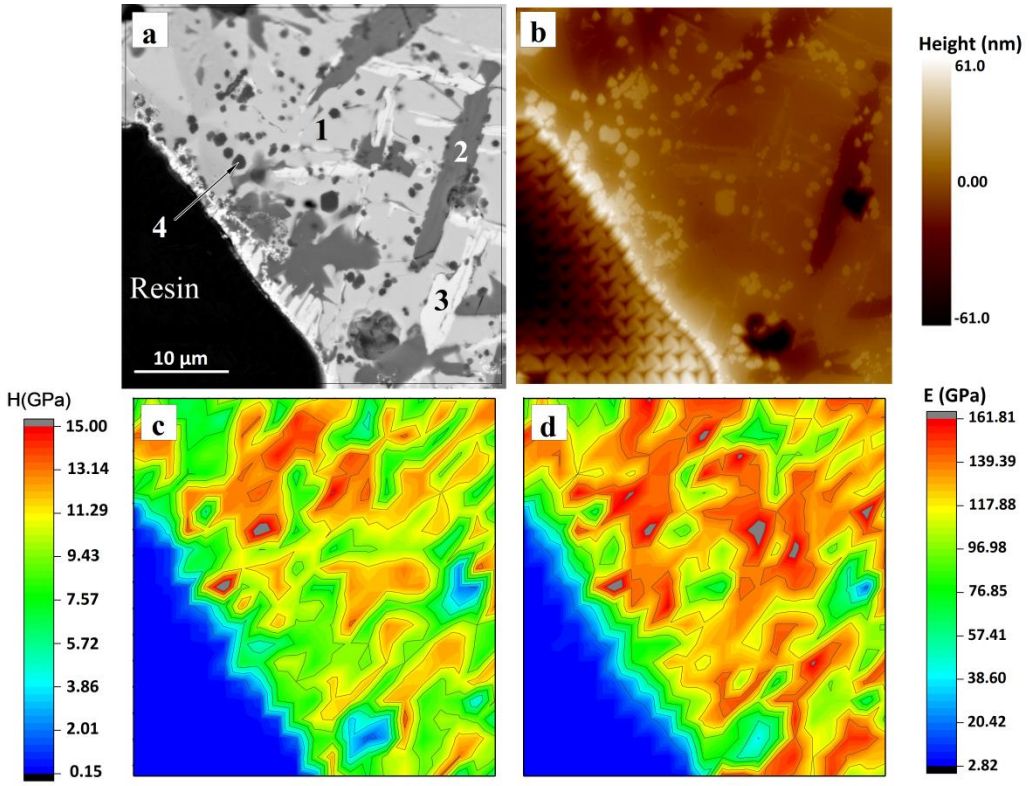

Fig. 2. a) BSE-SEM image and contour plots of b) topography, c) hardness *H* and d) elastic modulus *E* of as-sintered glass-ceramic G.

Table 3. Elastic modulus (*E*) and hardness (*H*) of different phases (F_{max} = 1 mN)

#	Phase	*E* (GPa)	*H* (GPa)	*CTE* (10^{-6} K^{-1})	Ref.
1	$BaCa_2Si_3O_9$	140 ± 18	12.2 ± 1.7	11.7 (100 – 800 ºC)	[35]
2	$CaSiO_3$	133 ± 9	9.5 ± 0.4	6 (20 – 300 ºC)	[36]
				9.4 (20 – 200 ºC)	[37]
				11.2 (100 – 800 ºC)	[35]
3	$BaSi_2O_5$	114 ± 15	10.6 ± 0.5	14.1 (20 – 1000 ºC)	[37]
4	SiO_2	105 ± 12	13.6 ± 0.2	< 1.5 (100 – 800 ºC)	[38]

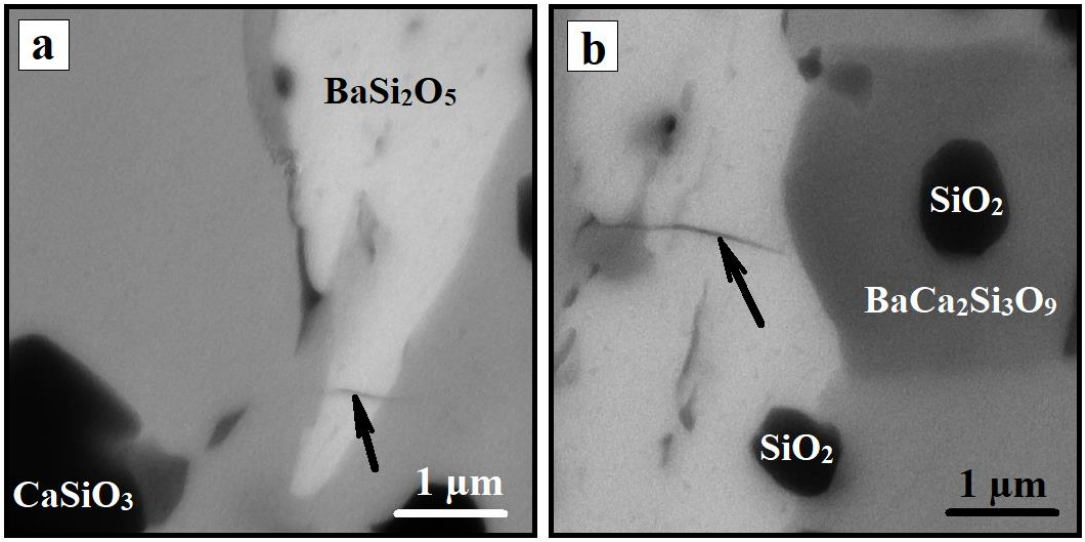

Fig. 3. Micro-cracks a) in a stress concentration zone and b) at a thin section of $BaSi_2O_5$ phase. The phases were identified by EDS.

Figure 4 shows that the measured hardness values decrease with increasing indentation load (F_{max}). This load-dependency of the hardness in low-load indentation testing is often associated with an indentation size effect (ISE) [39]. Several possible theoretical explanations have been proposed for the origin of the ISE such as the sensitivity of the load cell and intrinsic structural factors of the test materials [40]. The elastic modulus is constant at around 500 mN and deviations are within the limits of standard deviation in the considered load range. The slightly lower value for the lowest load might be a result of tip rounding (lack of calibration accuracy) or a surface roughness effect. However, a lower *E* value is measured when changing the indentation load from 0.5 N to 1 N, similar to the effect reflected in the hardness for this load range. For larger indentation sizes, the result is more affected by native micro-cracks and pores, hence, as the indentation load is increased, more discontinuities inevitably contribute to the measured *H* and *E* and decrease their values.

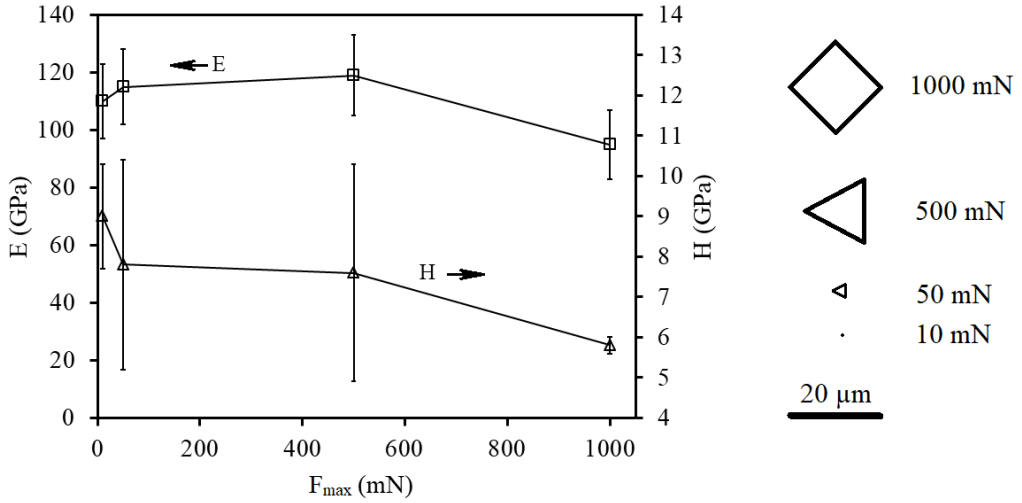

Fig. 4. Elastic modulus (*E*) and hardness (*H*) of the as-sintered glass-ceramic G as a function of applied load. The average indentation size for each F_{max} is shown schematically.

It can be seen in Table 4 that there is a tendency for a slight decrease in the elastic modulus after the long-term annealing. Continuing crystallization during annealing can lead to an increase in discontinuity density [41] or due to crystallization associated shrinkage, a slight increase in micro-pores, that subsequently decreases the elastic modulus [34]. However, it can be seen that the changes are within the limit of experimental uncertainties.

It can also be seen from Table 4 that the *E* values measured by impulse excitation and 1 N-load indentation are very close to each other. This implies that higher indentation loads are more suitable for *E* measurement because the tested volume is large enough to be representative of all phases and undulations. However, the results of the three-point bending test (3PB) are significantly lower than those of the other test methods. Also, the 3PB test indicates a stronger decrease in *E* after annealing. Contrary to the 3PB method [42], the unloading curve is normally used to estimate the elastic modulus in indentation testing [29]. Hence, the 3PB measurement during loading might lead to a decrease in actual values due to non-elastic effects, i.e. it can lead to a decrease in the apparent property due to micro-crack opening. There was also a slight variation (± 7 µm) in the thickness of the bars along their length, which may in addition cause

the bars to twist during 3PB testing. These added displacements also decrease the apparent elastic modulus. However, some of the uncertainty in 3PB test results is also systematic because the slope of the load-displacement line is very sensitive to the precision of the displacement measurement device.

Table 4. Elastic modulus (E) of glass-ceramic G for the as-sintered and annealed state as measured by different methods.

Method	Condition	Number of tests	E (GPa)*	Reference
Indentation (F_{max} =1 N)	As-sintered	21	95 ± 12	
	Annealed	21	94 ± 15	
Impulse excitation technique	As-sintered	1	99.1 ± 0.7	[26]
	Annealed	1	94.5 ± 0.6	
Three-point bending (3PB)	As-sintered	3	79 ± 17	[41]
	Annealed	1	70 ± 18	

*The squared model has been used to combine the systematic and random uncertainties [43,44].

Regarding the fracture toughness assessment, loads below 1 N did not induce a visible crack around the imprint. Therefore, another test machine (Micromet), which could apply higher loads, was utilized to evaluate the fracture toughness (K_{IC}) of the material. Depending on the shape of indentation-induced cracks, different relationships have been suggested in the literature to determine the fracture toughness. Figure 5 shows the top view around a Vickers indent, in which a and l are half indentation diagonal and length of the apparent Palmqvist-type cracks, respectively. According to Niihara et al. [45], a Palmqvist-type crack can be assumed when the l/a ratio is lower than 2.5, otherwise a median (half-penny) crack is suggested to exist. In this study, most indentations (like the one illustrated in Fig. 5) created a Palmqvist-type crack. Figure 6 presents the measured K_{IC} for different F_{max}. The uncertainty in determining the types of some cracks could have caused a larger scatter in K_{IC} values for this load. However, Niihara et al. [45]

suggested that high loads are not required, as long as it can be recognized that the observed cracks have the geometry of the Palmqvist crack.

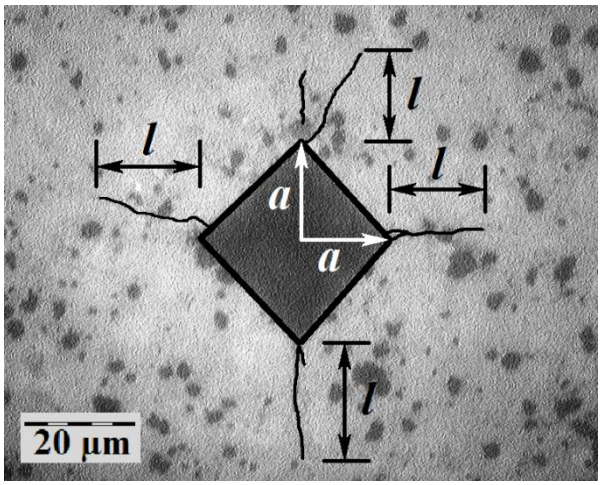

Fig. 5. Optical micrograph of an indentation imprint (F_{max} = 3 N). The cracks have been highlighted to enhance visibility.

Figure 6 also compares the H measured using different testing machines for different F_{max}. As mentioned above, the reduction of hardness with increasing F_{max} can be associated with the ISE as well as more contribution of micro-cracks and local porosity. A slight tendency for increased measured hardness values with increasing load from 3 N to 10 N can be seen in Fig. 6. This phenomenon, a so-called reversed indentation size effect (RISE), can be associated with indentation-induced cracking. During indenting, a fraction of load and associated energy is consumed in the opening of the indentation induced cracks. Therefore, a smaller indentation imprint and then higher apparent hardness are expected [46].

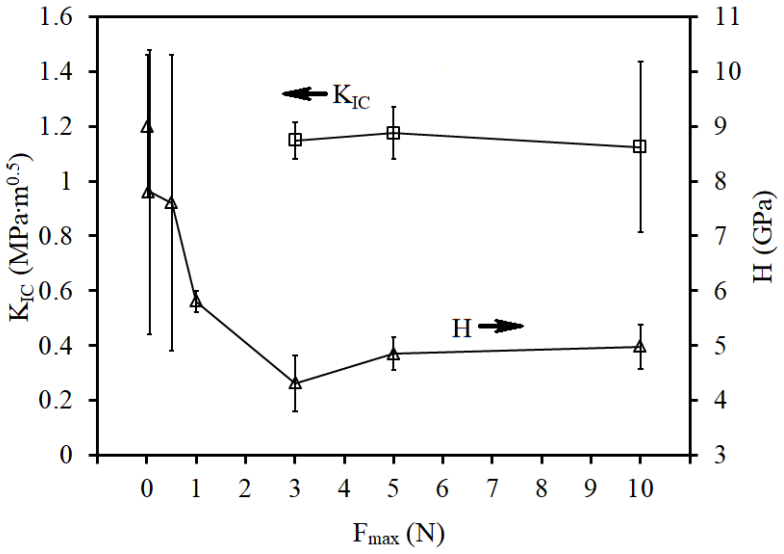

Fig. 6. Fracture toughness (K_{IC}) and hardness (H) of as-sintered glass-ceramic G measured with F_{max} = 0.01-10 N.

Figure 7 compares the fracture toughness (K_{IC}) and hardness (H) of different sealing materials developed at Forschungszentrum Jülich. The sealant B is a fully crystallized glass with a similar Ba:Ca:Si ratio to the sealant G but the less additive content [27]. The sealants H-P, H-Ag and H-F are partially crystallized composites based on glass composition H reinforced with yttria-stabilized zirconia (YSZ) particles, silver particles and YSZ fibers, respectively [33]. As can be seen, although the annealing does not cause much change in the hardness, however, it significantly increases K_{IC} of the partially crystallized sealant. Continuing crystallization during annealing increases the volume fraction of ceramic phases in these sealants and consequently enhances their resistance to crack growth. However, sealant G shows a relatively stable K_{IC} and H in terms of any effect related to a potential aging process. Besides, sealant G in as-sintered and annealed states has a K_{IC} of 1.15 ± 0.18 MPa·m$^{0.5}$ and 1.23 ± 0.21 MPa·m$^{0.5}$, respectively, which are near that of the composite sealing materials.

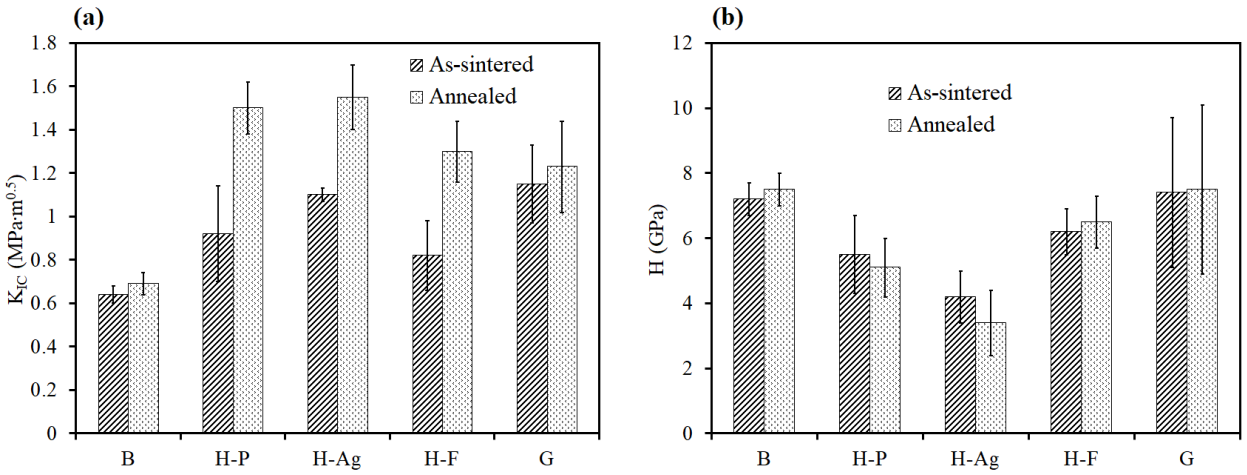

Fig. 7. A comparison of a) fracture toughness and b) hardness values of glass-ceramic G with that of other sealing materials developed at Forschungszentrum Jülich [33]. The values of K_{IC} and H are measured with an F_{max} of 3-10 N and 10-1000 mN, respectively.

Complementary SEM investigations revealed that crystallized phases and pre-existing micro-cracks can effectively deflect or stop indentation-induced cracks (Fig. 8b). Such a crack deflection leads also to a change in the loading mode at the tip of crack from pure opening (I) to other modes. In brittle material, the crack growth under modes II, III or mixed-mode is more difficult than pure mode I. Also, compared with straight crack, the deflected crack must proceed to a longer distance to reach a given macroscopic crack length (l). Therefore, crack deflection is expected to increase fracture toughness. Figure 8c shows crack branching as another potential toughening mechanism observed for sealant G. This mechanism leads to a decrease in stress intensity factor at the tip of the crack by dividing the crack-opening displacement between the branches. The branches can originate from the pre-existing micro-cracks. In conclusion, the presence of micro-stresses and micro-cracks in glass-ceramic G has a positive effect on its fracture toughness.

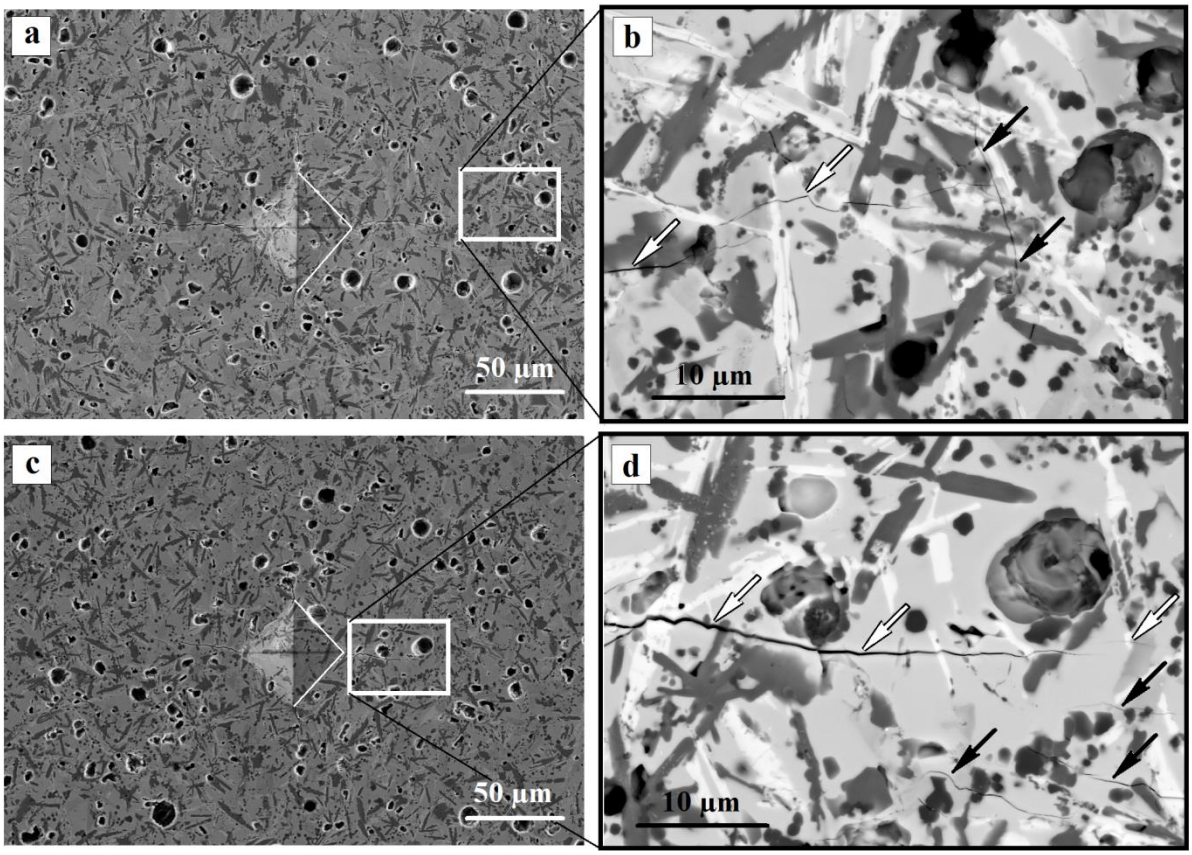

Fig. 8. BSE-SEM images of indented surface with F_{max} = 10 N; a) and b) crack deflection, c) and d) crack branching. The white and black arrows indicate indentation-induced cracks and pre-existing micro-cracks, respectively.

Figure 9 shows indentation cracks after additional heat treatment of 70 h at 850 ºC. Figures 9b and 9c indicate a zone in which the crack has been healed. The sharp edges become more visible in Fig. 9d due to the used In-Beam SE detector. The lower brightness of an individual section of a crack implies that the edges are rounded and the gap is filled in that area. Some faceted crystals protruding from the surface are also observed at higher magnification (Fig. 10). They may be ceramic phases which have continued to grow or have been moved due to the low viscosity glassy phases at high temperature. These findings can be evidence of viscous flow and a self-healing ability of the apparently fully crystallized sealant G at elevated temperatures. Regarding the long-time operation of SOCs at high temperature and the presence of a dead load

on the stack components, more discontinuities might be expected to be potentially healed by the viscous flow driven associated with capillarity forces of residual glassy phases as well as residual stresses caused by mechanical impact [47,48]. In other words, the clamping load and the weight of the upper layers in the stack are expected to accelerate the crack healing process, especially if the temperature increases locally because of direct contact of fuel and oxidant gases. However, it may not be a promising method for repairing the large-scale crack such as a failed joint.

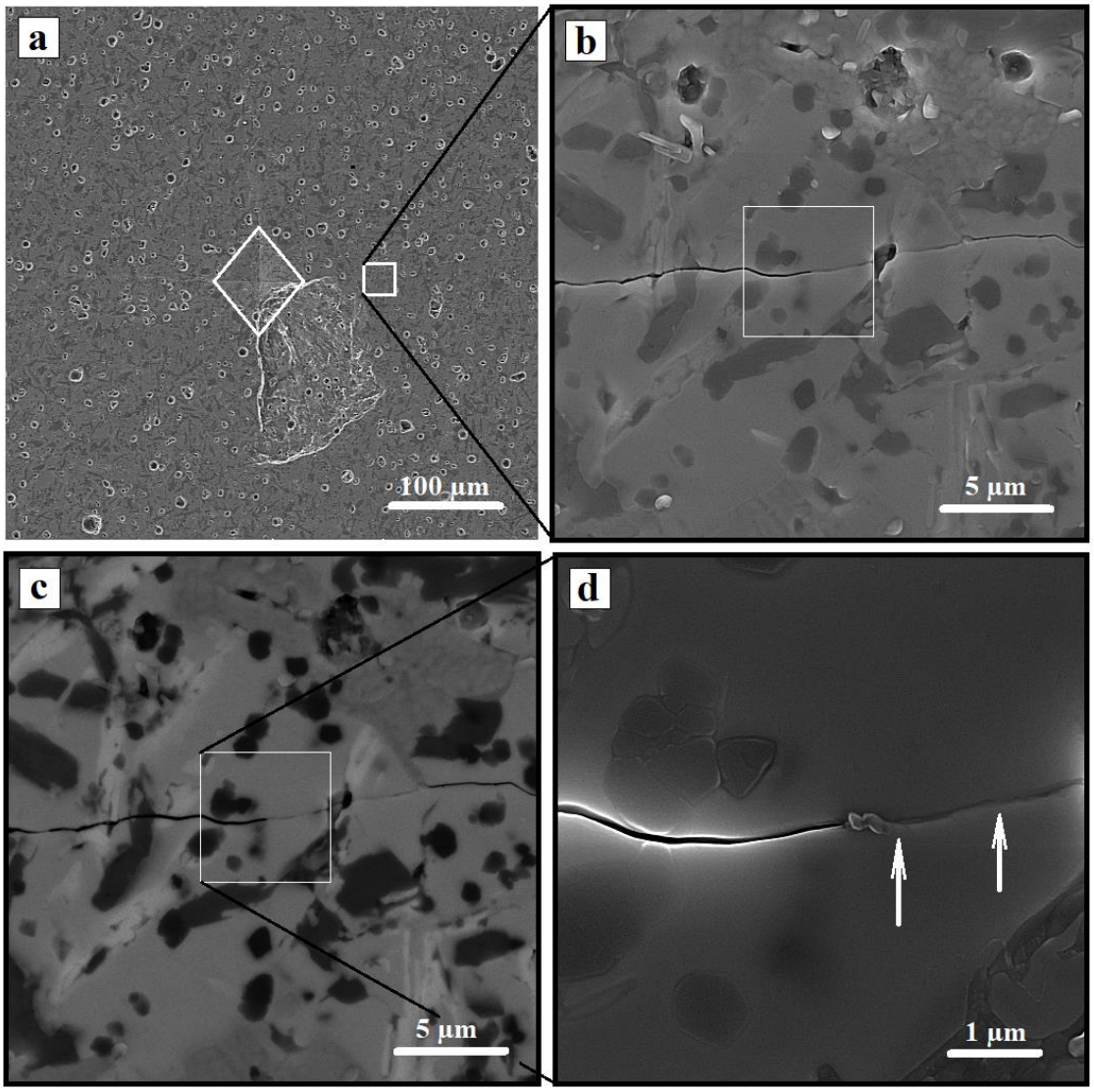

Fig. 9. a) SE-SEM image of indented surface with F_{max} = 10 N after heat treating for 70 h at 850 ºC, b) SE-SEM and c) BSE-SEM image of indicated area in (a), d) In-Beam image of indicated area in (c).

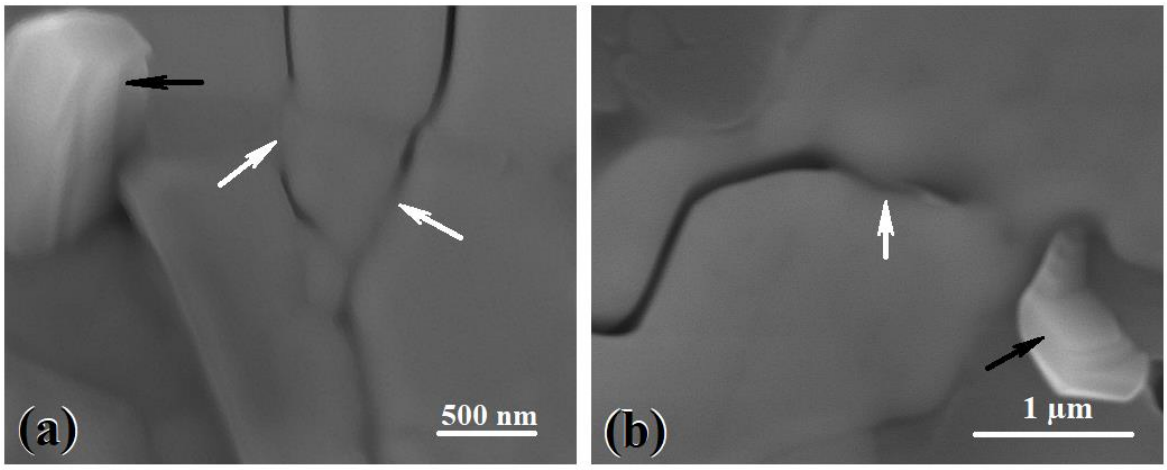

Fig. 10. SE-SEM images of indented surface with F_{max} = 10 N after heat treating for 70 h at 850 ºC; a) middle and b) tip of indentation crack. The white and black arrows indicate the healed zone and protruded phases, respectively.

As can be seen in Fig. 10, the crack path has not been continuously healed, which has also been observed by Abdoli et al. [49] for another glass-ceramic sealant. This is likely to be due to the presence of crystalline phases that reduce access to glassy phases. However, four phenomenological stages suggested by Hrma et al. [47], i.e. (i) relaxation and blunting, (ii) receding and breaking up, (iii) rounding and grooving (iv) and smoothing and spheroidizing, were not sequentially seen during the self-healing of the glass-ceramic G. Instead, all the steps were captured simultaneously in the micrograph.

4. Conclusions

In this study, an indentation test method was utilized to evaluate the mechanical behavior of a glass-ceramic sealant on a micro-scale. The observations can be summarized as follows:

- The measured values for elastic modulus (E) and hardness (H) depend on the indentation load (F_{max}). The magnitude of F_{max} should be high enough so that the

affecting volume is a suitable sample of all material and also low enough to prevent the cracking around the indentation imprint.

- The elastic moduli (E) measured by the indentation method using a load of 1 N were close to the value obtained by the impulse excitation technique, which is considered to be a reliable method to derive the macroscopic elastic modulus of materials.
- The fracture toughness (K_{IC}) of sealant G is close to that of the composite sealing materials. Also, compared with reinforced partially crystallized glasses, material G shows a relatively stable K_{IC} in terms of the effect of a thermal aging process.
- Pre-existing microcracks in sealant G play an important role in stopping, deflecting and branching the cracks and consequently appear to increase its fracture toughness.
- Although the sealant G is considered to be a fully crystallized glass, it is still able to heal the micro-cracks by the viscous flow and capillary forces of residual glassy phases. In the stack, the sealant sandwiched between the other components is under compressive residual stress which could accelerate the crack healing process upon the stack reheating and decrease the impact of thermal cycles.

Acknowledgements

The authors wish to thank Mr. D. Federmann and Ms. T. Osipova for the support in specimens' preparations and testing, Dr. E. Wessel and Dr. D. Grüner for SEM investigations, and Prof. L. Singheiser and Prof. M. Krüger for hosting at Forschungszentrum Jülich. The authors also express their gratitude to the Ministry of Science, Research and Technology of Iran, Iran's National Elites Foundation, Sharif University of Technology and Niroo Research Institute (NRI) for financial support and providing a part of the research facilities.

References

[1] M. Kaur, G. Kaur, V. Kumar, Understanding intermediate temperature solid oxide fuel cells, in: Intermed. Temp. Solid Oxide Fuel Cells, Elsevier, 2020: pp. 1–32. doi:10.1016/B978-0-12-817445-6.00001-6.

[2] A. Selçuk, A. Atkinson, Measurement of Mechanical Strength of Glass-to-Metal Joints, Fuel Cells. 15 (2015) 595–603. doi:10.1002/fuce.201500028.

[3] V. Kumar, M. Kaur, G. Kaur, S.K. Arya, G. Pickrell, Stacking designs and sealing principles for IT-solid oxide fuel cell, in: Intermed. Temp. Solid Oxide Fuel Cells, Elsevier, 2020: pp. 379–410. doi:10.1016/B978-0-12-817445-6.00011-9.

[4] M. Fakouri Hasanabadi, J. Malzbender, S.M. Groß-Barsnick, H. Abdoli, A.H. Kokabi, M.A. Faghihi-Sani, Finite element optimization of sample geometry for measuring the torsional shear strength of glass/metal joints, Ceram. Int. 46 (2020) 4857–4863. doi:10.1016/j.ceramint.2019.10.221.

[5] M. Ferraris, V. Casalegno, F. Smeacetto, M. Salvo, Glass as joining material for ceramic matrix composites: 25 years of research at Politecnico di Torino, Int. J. Appl. Glas. Sci. (2020) ijag.15032. doi:10.1111/ijag.15032.

[6] H. Mousa Mirabad, A. Nemati, M.A. Faghihi-Sani, M. Fakouri Hasanabadi, H. Abdoli, Effect of YSZ sol-gel coating on interaction of Crofer22 APU with sealing glass for solid oxide fuel/electrolysis cell, J. Alloys Compd. 847 (2020) 156496. doi:10.1016/j.jallcom.2020.156496.

[7] M. Peksen, A coupled 3D thermofluid–thermomechanical analysis of a planar type production scale SOFC stack, Int. J. Hydrogen Energy. 36 (2011) 11914–11928. doi:10.1016/j.ijhydene.2011.06.045.

[8] L. Blum, Q. Fang, S.M. Groß-Barsnick, L.G.J. (Bert) de Haart, J. Malzbender, N.H. Menzler, W.J. Quadakkers, Long-term operation of solid oxide fuel cells and preliminary findings on accelerated testing, Int. J. Hydrogen Energy. 45 (2020) 8955–8964. doi:10.1016/j.ijhydene.2020.01.074.

[9] N.P. Brandon, E. Ruiz-Trejo, P. Boldrin, Solid Oxide Fuel Cell Lifetime and Reliability, Academic Press, London, UK, 2017.

[10] S.-M. Gross-Barsnick, Interaction of glass-ceramic sealants with solid oxide fuel cell components: thermo-mechanical analysis, in: Intermed. Temp. Solid Oxide Fuel Cells, Elsevier, 2020: pp. 411–426. doi:10.1016/B978-0-12-817445-6.00012-0.

[11] M. Fakouri Hasanabadi, A.H. Kokabi, A. Nemati, S. Zinatlou Ajabshir, Interactions near the triple-phase boundaries metal/glass/air in planar solid oxide fuel cells, Int. J. Hydrogen Energy. 42 (2017) 5306–5314. doi:10.1016/j.ijhydene.2017.01.065.

[12] H. Abdoli, P. Alizadeh, D. Boccaccini, K. Agersted, Fracture toughness of glass sealants for solid oxide fuel cell application, Mater. Lett. 115 (2014) 75–78.

doi:10.1016/j.matlet.2013.10.013.

[13] J. Malzbender, Y. Zhao, T. Beck, Fracture and creep of glass–ceramic solid oxide fuel cell sealant materials, J. Power Sources. 246 (2014) 574–580. doi:10.1016/j.jpowsour.2013.08.010.

[14] J. Malzbender, Y. Zhao, Micromechanical testing of glass–ceramic sealants for solid oxide fuel cells, J. Mater. Sci. 47 (2012) 4342–4347. doi:10.1007/s10853-012-6286-5.

[15] J. Malzbender, Y. Zhao, Flexural strength and viscosity of glass ceramic sealants for solid oxide fuel cell stacks, Fuel Cells. 12 (2012) 47–53. doi:10.1002/fuce.201100116.

[16] T. Osipova, J. Wei, G. Pećanac, J. Malzbender, Room and elevated temperature shear strength of sealants for solid oxide fuel cells, Ceram. Int. 42 (2016) 12932–12936. doi:10.1016/j.ceramint.2016.05.064.

[17] B. Cela Greven, S.M. Gross-Barsnick, D. Federmann, R. Conradt, Strength evaluation of multilayer glass-ceramic sealants, Fuel Cells. 13 (2013) 565–571. doi:10.1002/fuce.201200155.

[18] H. Javed, A. Sabato, I. Dlouhy, M. Halasova, E. Bernardo, M. Salvo, K. Herbrig, C. Walter, F. Smeacetto, Shear Performance at Room and High Temperatures of Glass–Ceramic Sealants for Solid Oxide Electrolysis Cell Technology, Materials (Basel). 12 (2019) 298. doi:10.3390/ma12020298.

[19] T. Altan, S. Celik, Effect of surface roughness of the metallic interconnects on the bonding strength in solid oxide fuel cells, Int. J. Hydrogen Energy. (2020). doi:10.1016/j.ijhydene.2020.03.136.

[20] K.-Y. Chen, C.-K. Lin, S.-H. Wu, C.-K. Liu, R.-Y. Lee, Thermo-Mechanical Fatigue of SOFC Glass-Ceramic Sealant/Steel Interconnect Joint in a Reducing Atmosphere, ECS Trans. 91 (2019) 2323–2329. doi:10.1149/09101.2323ecst.

[21] M. Fakouri Hasanabadi, A.H. Kokabi, M.A. Faghihi-Sani, S.M. Groß-Barsnick, J. Malzbender, Room- and high-temperature torsional shear strength of solid oxide fuel/electrolysis cell sealing material, Ceram. Int. 45 (2019) 2219–2225. doi:10.1016/j.ceramint.2018.10.134.

[22] W. Höland, G.H. Beall, Glass-Ceramic Technology, 2nd ed, John Wiley & Sons, Inc., Hoboken, NJ, USA, 2012. doi:10.1002/9781118265987.

[23] K.S. Weil, The state-of-the-art in sealing technology for solid oxide fuel cells, JOM. 58 (2006) 37–44. doi:10.1007/s11837-006-0052-6.

[24] M.K. Mahapatra, K. Lu, Glass-based seals for solid oxide fuel and electrolyzer cells – A review, Mater. Sci. Eng. R Reports. 67 (2010) 65–85. doi:10.1016/j.mser.2009.12.002.

[25] J.W. Fergus, Sealants for solid oxide fuel cells, J. Power Sources. 147 (2005) 46–57. doi:10.1016/j.jpowsour.2005.05.002.

[26] M. Fakouri Hasanabadi, M.A. Faghihi-Sani, A.H. Kokabi, S.M. Groß-Barsnick, J. Malzbender, Room- and high-temperature flexural strength of a stable solid oxide

fuel/electrolysis cell sealing material, Ceram. Int. 45 (2019) 733–739. doi:10.1016/j.ceramint.2018.09.236.

[27] S.-M. Groß, U. Reisgen, Glaslöten - eine anspruchsvolle Fügetechnik nicht nur für die Hochtemperatur-Brennstoffzelle, Schweißen Und Schneid. 59 (2007) 70–7. http://juser.fz-juelich.de/record/56112.

[28] M. Fakouri Hasanabadi, M.A. Faghihi-Sani, A.H. Kokabi, J. Malzbender, The analysis of torsional shear strength test of sealants for solid oxide fuel cells, Ceram. Int. 43 (2017) 12546–12550. doi:10.1016/j.ceramint.2017.06.128.

[29] W.C. Oliver, G.M. Pharr, An improved technique for determining hardness and elastic modulus using load and displacement sensing indentation experiments, J. Mater. Res. 7 (1992) 1564–1583. doi:10.1557/JMR.1992.1564.

[30] ASTM C1327-15, Standard Test Method for Vickers Indentation Hardness of Advanced Ceramics, ASTM International, West Conshohocken, PA, USA, 2015. doi:10.1520/C1327-15.

[31] A. Chanda, B.X. Huang, J. Malzbender, R.W. Steinbrech, Micro- and macro-indentation behaviour of Ba0.5Sr0.5Co0.8Fe0.2O3-d perovskite, J. Eur. Ceram. Soc. 31 (2011) 401–408. doi:10.1016/j.jeurceramsoc.2010.10.022.

[32] G.D. Quinn, R.C. Bradt, On the vickers indentation fracture toughness Test, J. Am. Ceram. Soc. 90 (2007) 673–680. doi:10.1111/j.1551-2916.2006.01482.x.

[33] Y. Zhao, J. Malzbender, S.M. Gross, The effect of room temperature and high temperature exposure on the elastic modulus, hardness and fracture toughness of glass ceramic sealants for solid oxide fuel cells, J. Eur. Ceram. Soc. 31 (2011) 541–548. doi:10.1016/j.jeurceramsoc.2010.10.032.

[34] S. Rodríguez-López, J. Malzbender, V.M. Justo, F.C. Serbena, S.M. Groß-Barsnick, M.J. Pascual, Thermo-Mechanical Stability and Gas-Tightness of Glass-Ceramics Joints for SOFC in the System MgO-BaO/SrO-B2O3-SiO2, Front. Mater. 7 (2020) 1–15. doi:10.3389/fmats.2020.00019.

[35] M. Kerstan, M. Müller, C. Rüssel, Binary, ternary and quaternary silicates of CaO, BaO and ZnO in high thermal expansion seals for solid oxide fuel cells studied by high-temperature X-ray diffraction (HT-XRD), Mater. Res. Bull. 46 (2011) 2456–2463. doi:10.1016/j.materresbull.2011.08.031.

[36] N.H. Menzler, M. Bram, H.P. Buchkremer, D. Stöver, Development of a gastight sealing material for ceramic components, J. Eur. Ceram. Soc. 23 (2003) 445–454. doi:10.1016/S0955-2219(02)00097-3.

[37] S.K. Weil, J.E. Deibler, J.S. Hardy, D.S. Kim, G.-G. Xia, L. a. Chick, C. a. Coyle, Rupture Testing as a Tool for Developing Planar Solid Oxide Fuel Cell Seals, J. Mater. Eng. Perform. 13 (2004) 316–326. doi:10.1361/10599490419306.

[38] A.H.A. Pereira, D.Y. Miyaji, M.D. Cabrelon, J. Medeiros, J.A. Rodrigues, A study about

the contribution of the α-β phase transition of quartz to thermal cycle damage of a refractory used in fluidized catalytic cracking units, Cerâmica. 60 (2014) 449–456. doi:10.1590/S0366-69132014000300019.

[39] J. Gong, J. Wu, Z. Guan, Examination of the indentation size effect in low-load vickers hardness testing of ceramics, J. Eur. Ceram. Soc. 19 (1999) 2625–2631. doi:10.1016/S0955-2219(99)00043-6.

[40] D. Jiang, Recent progresses in the phenomenological description for the indentation size effect in microhardness testing of brittle ceramics, J. Adv. Ceram. 1 (2012) 38–49. doi:10.1007/s40145-012-0004-2.

[41] M. Fakouri Hasanabadi, Investigation of mechanical properties of glass-ceramic sealant for solid oxide fuel/electrolysis cells, Sharif University of Technology, Tehran, Iran, 2018. doi:10.13140/RG.2.2.15805.72161/3.

[42] DIN EN 843-2: 2007-03, Advanced technical ceramics - Mechanical properties of monolithic ceramics at room temperature - Part 2: Determination of Young's modulus, shear modulus and Poisson's ratio, 2007.

[43] K.C. Crandall, R.W. Seabloom, Engineering fundamentals: in measurements, probability, statistics, and dimensions, McGraw-Hill, New York, New York, United States, 1970.

[44] P.H. Petersen, D. Stöckl, J.O. Westgard, S. Sandberg, K. Linnet, L. Thienpont, Models for Combining Random and Systematic Errors. Assumptions and Consequences for different Models, Clin. Chem. Lab. Med. 39 (2001) 589–595. doi:10.1515/CCLM.2001.094.

[45] K. Niihara, R. Morena, D.P.H. Hasselman, Evaluation of KIc of brittle solids by the indentation method with low crack-to-indent ratios, J. Mater. Sci. Lett. 1 (1982) 13–16. doi:10.1007/BF00724706.

[46] H. Li, R.C. Bradt, The effect of indentation-induced cracking on the apparent microhardness, J. Mater. Sci. 31 (1996) 1065–1070. doi:10.1007/BF00352908.

[47] P. Hrma, W.T. Han, A.R. Cooper, Thermal healing of cracks in glass, J. Non. Cryst. Solids. 102 (1988) 88–94. doi:10.1016/0022-3093(88)90116-0.

[48] W. LIU, X. SUN, M. KHALEEL, Predicting Young's modulus of glass/ceramic sealant for solid oxide fuel cell considering the combined effects of aging, micro-voids and self-healing, J. Power Sources. 185 (2008) 1193–1200. doi:10.1016/j.jpowsour.2008.07.017.

[49] H. Abdoli, P. Alizadeh, D. Boccaccini, K. Agersted, Effects of thermal aging on thermo-mechanical behavior of a glass sealant for solid oxide cell applications, J. Eur. Ceram. Soc. 34 (2014) 2525–2534. doi:10.1016/j.jeurceramsoc.2014.02.004.